Retrieval of forest canopy attributes based on a geometric-optical model using airborne LiDAR and optical remote-sensing data

Chunxiang Cao [a], Yunfei Bao [a b], Min Xu [a c], Wei Chen [a c], Hao Zhang [a], Qisheng He [a c], Zengyuan Li [d], Huadong Guo [e], Jiahong Li [f], Xiaowen Li [a] & Guanghe Li [g]

[a] State Key Laboratory of Remote Sensing Science, Jointly Sponsored by the Institute of Remote Sensing Applications of the Chinese Academy of Sciences and Beijing Normal University, Beijing, 100101, PR China

[b] Beijing Institute of Space Mechanics and Electricity, Beijing, 100076, PR China

[c] Graduate School of the Chinese Academy of Sciences, Beijing, 100049, PR China

[d] Research Institute of Forest Resources and Information Techniques, Chinese Academy of Forestry, Beijing, 10009, PR China

[e] Centre for Earth Observation and Digital Earth, Chinese Academy of Sciences, Beijing, 100190, PR China

[f] National Remote-sensing Centre of China, Beijing, 100862, PR China

[g] Department of Industry Design, College of Architecture and Urban Planning, Beijing University of Technology, Beijing, 100124, PR China

Available online: 18 Nov 2011

Taylor & Francis
Taylor & Francis Group

Retrieval of forest canopy attributes based on a geometric-optical model using airborne LiDAR and optical remote-sensing data

CHUNXIANG CAO*†, YUNFEI BAO†‡, MIN XU†§, WEI CHEN†§,
HAO ZHANG†, QISHENG HE†§, ZENGYUAN LI¶, HUADONG GUO|,
JIAHONG LI††, XIAOWEN LI† and GUANGHE LI‡‡

†State Key Laboratory of Remote Sensing Science, Jointly Sponsored by the Institute of Remote Sensing Applications of the Chinese Academy of Sciences and Beijing Normal University, Beijing 100101, PR China
‡Beijing Institute of Space Mechanics and Electricity, Beijing 100076, PR China
§Graduate School of the Chinese Academy of Sciences, Beijing 100049, PR China
¶Research Institute of Forest Resources and Information Techniques, Chinese Academy of Forestry, Beijing 10009, PR China
|Centre for Earth Observation and Digital Earth, Chinese Academy of Sciences, Beijing 100190, PR China
††National Remote-sensing Centre of China, Beijing 100862, PR China
‡‡Department of Industry Design, College of Architecture and Urban Planning, Beijing University of Technology, Beijing 100124, PR China

In the retrieval of forest canopy attributes using a geometric-optical model, the spectral scene reflectance of each component should be known as prior knowledge. Generally, these reflectances were acquired by a foregone survey using an analytical spectral device. This article purposed to retrieve the forest structure parameters using light detection and ranging (LiDAR) data, and used a linear spectrum decomposition model to determine the reflectances of the spectral scene components, which are regarded as prior knowledge in the retrieval of forest canopy cover and effective plant area index (PAI_e) using a simplified Li–Strahler geometric-optical model based on a Satellites Pour l'Observation de la Terre 5 (SPOT-5) high-resolution geometry (HRG) image. The airborne LiDAR data are first used to retrieve the forest structure parameters and then the proportion of the SPOT pixel not covered by crown or shadow K_g of each pixel in the sample was calculated, which was used to extract the reflectances of the spectral scene components by a linear spectrum decomposition model. Finally, the forest canopy cover and PAI_e are retrieved by the geometric-optical model. As the acquired time of SPOT-5 image and measured data has a discrepancy of about 2 months, the retrieved result of forest canopy cover needs a further validation. The relatively high value of R^2 between the retrieval result of PAI_e and the measurements indicates the efficiency of our methods.

1. Introduction

Retrieval of forest structural attributes using remote-sensing data is a hotspot in the field of forest remote sensing. Canopy cover and effective plant area index (PAI_e) are the two key forest canopy attributes which can contribute to the monitoring

*Corresponding author. Email: cao413@irsa.ac.cn

of forest health. Various remote-sensing data such as optical image, light detection and ranging (LiDAR) and synthetic aperture radar (SAR) have been used in the retrieval to forest canopy attributes. No matter which remote-sensing data were used, the common approaches to forest canopy attributes can be divided into two types: methods based on empirical regression and methods based on models. Both of these methods have the problem of mixed pixels. Mixed pixels have serious effects on the retrieval precision of forest canopy attributes. Many errors may be induced if one retrieves the forest canopy attributes directly from the mixed spectrum (Hu *et al*. 2004). Therefore, the decomposition of the mixed spectrum from passive sensors is a very important step to improve the precision of retrieval parameters of mixed pixels. With the development of mixed pixel decomposition theory, many decomposition models of mixed pixels such as the linear model, probabilistic model, geometric-optical model, stochastic geometry model and fuzzy analysis have been exploited. The geometric-optical models have been proved to effectively retrieve the canopy cover (Franklin and Strahler 1988, Franklin and Turner 1992, Chopping *et al*. 2006, 2008) and leaf area index (LAI) (Hall *et al*. 1995a,b, Hu *et al*. 2004). All these retrieval models were built based on prior knowledge of end members. In the retrieval of forest canopy attributes using the geometric-optical model, the spectral scene reflectance of each component should be known as prior knowledge. Generally, these reflectances were acquired by a foregone survey using an analytical spectral device. This article proposes to retrieve the forest structure parameters using LiDAR data, and uses a linear spectrum decomposition model to determine the reflectances of the spectral scene components, which are regarded as prior knowledge in the retrieval of forest canopy cover and PAI_e using a simplified Li–Strahler geometric-optical model. The airborne LiDAR data are first used to retrieve forest structure parameters, and then the proportion of the pixel not covered by crown or shadow K_g of each pixel in the sample is calculated, which is used to extract the reflectances of the spectral scene components by a linear spectrum decomposition model. Finally, the forest canopy cover and PAI_e are retrieved by the geometric-optical model.

2. The study area

The study area of Dayekou is situated in the Qilian Mountain area, with its geographic coordinates ranging from 38° 29′ to 38° 35′ N in latitude and from 100° 12′ to 100° 20′ E in longitude within Gansu province, western China (figure 1). The elevation varies from 2500 to 3800 m above sea level. The area has a temperate continental mountainous climate. In winter the atmospheric circulation is controlled by the Mongolia anticyclone, which results in cold and dry conditions and little precipitation. When the atmospheric circulation is controlled by the continental cyclone in summer, the diurnal difference of temperature is dramatic. The difference of precipitation between summer and winter is large, and the annual precipitation takes place mainly during summer. Influenced by the climate and terrain, the prevalent vegetation types in the study area are mountainous pastures and forests. The dominant vegetation includes *Picea crassifolia*, *Sabina przewalski* and grassland. Vegetation density varies with terrain, soil, water and climate factors. In this study, the coniferous tree species (*P. crassifolia*) was selected as a target.
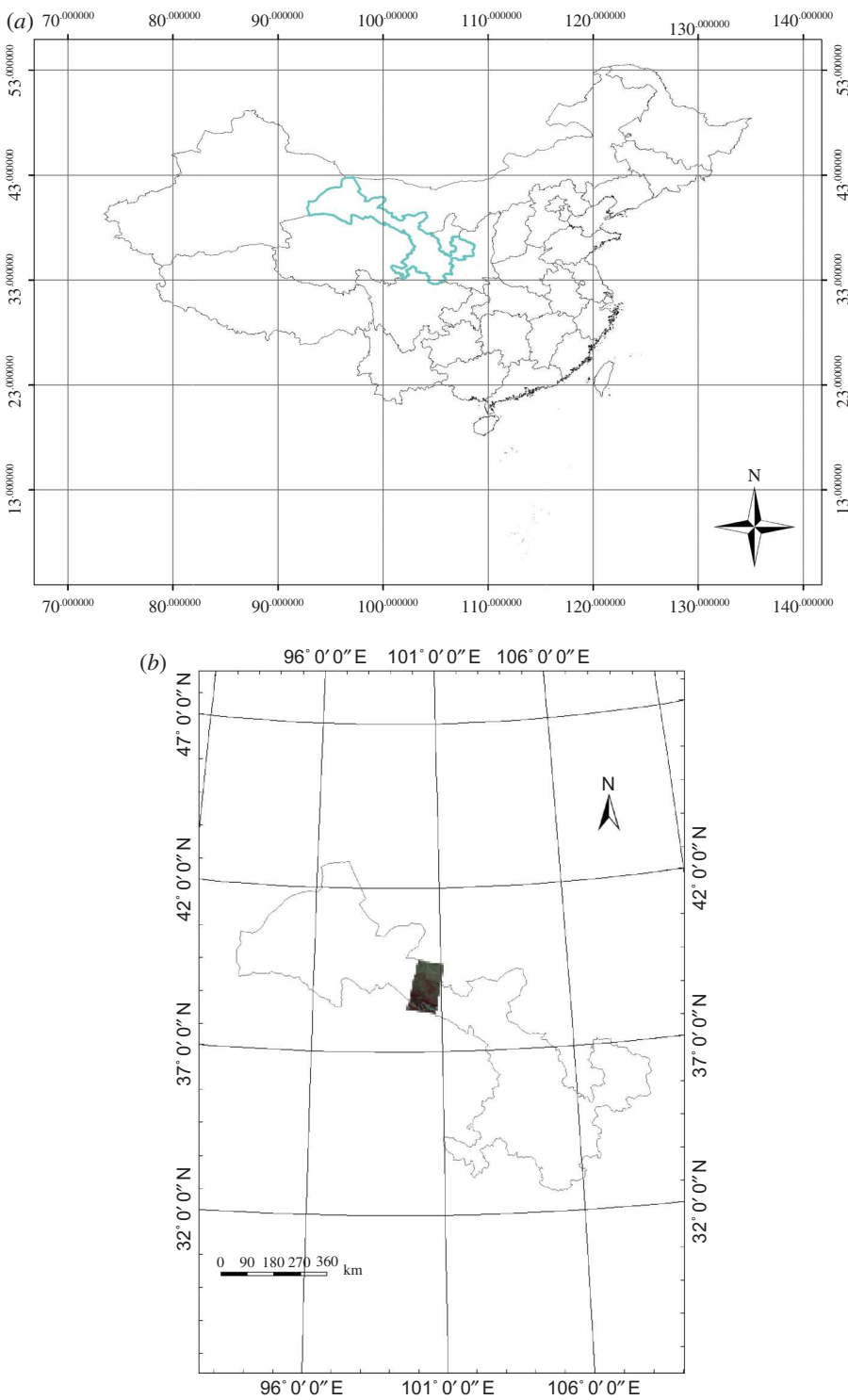
Figure 1.   The study area. (*a*) The site of Gansu province in China and (*b*) the site of Dayekou area in Gansu province.

3. Data and data preprocessing

3.1 *LiDAR data and preprocessing*

An airborne laser scan flight was carried out over the test area in June 2008. The airborne laser scan system used was LiteMapper-5600, developed by IGI (Kreuztal, Germany). It is one of the first commercial airborne LiDAR terrain mapping systems to use waveform digitization. Its laser scanner is RIEGL LMS-Q560. The sensor specifications are given in table 1.

The flight over the study area was conducted with a nominal height above ground of 700–800 m, leading to a pulse density of 0.36–1.6 points per square metre. To increase the pulse density, repetitive flight was carried out over the sample study area. The flights in the sample plot are five times more than those in other areas, so the pulse density was increased to 2–7 points per square metre. Additionally, as the laser scanner records waveform data, multiple returns need to be sampled. The site of the LiDAR data we acquired is shown in figure 2.

The processing of the airborne LiDAR data in the study area is divided into two parts. First is the orthorectification and topographic correction to the optical image. The Satellites Pour l'Observation de la Terre 5 (SPOT-5) image is processed using a digital elevation model (DEM) derived from the LiDAR data (the green area in figure 2). Second is the processing of the high-density LiDAR data (the blue area in figure 2) for the exact description of the ground. Therefore, the high-density LiDAR data are used to extract the individual tree parameters and create the forest canopy cover and PAI_e. In the preprocessing function, the ground points are separated from the vegetation points using the skewness change algorithm based on the intensity information of the high-density LiDAR data (Bao *et al*. 2008). After the separation of LiDAR points, a digital terrain model (DTM) and fractional vegetation cover are generated according to whether pulses have their first echo on the ground. The digital surface model (DSM) is obtained by filtering out the uppermost echoes and then the canopy height model (CHM) is obtained. Finally, based on the variational window (equation (1)), the local maximum filter method is used to extract individual tree height and crown width from the CHM (Popescu *et al*. 2002). The extracted vegetation cover, tree height and crown width of the sample area are then used for the synchronous retrieval of the forest canopy cover and PAI_e of the whole study area which is the key point of this article elaborated in the methodology:

$$D_{crown} = 0.2041 H_{tree} + 1.3457 \ (R^2 = 0.6103), \tag{1}$$

where D_{crown} is the crown width and H_{tree} is the tree height.

Table 1. Specifications of RIEGL LMS-Q560.

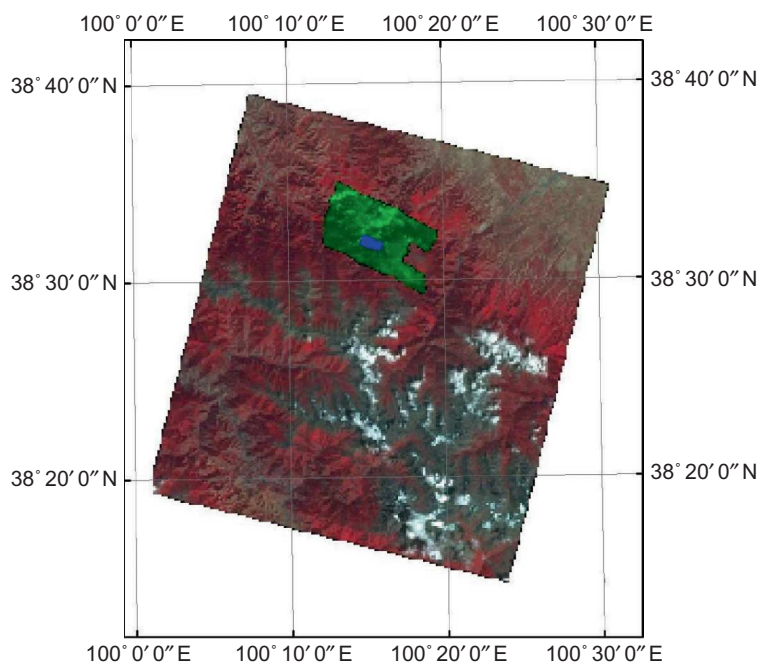|	
Maximum measurement range (m)	1800
Measurement accuracy (mm)	20
Maximum pulse repetition frequency (kHz)	200
Multiple target separation within single shot (m)	0.6
Laser wavelength (nm)	1550
Return pulse width resolution (m)	0.15
Scan speed (scans/s)	10–160
Scan angle accuracy (°)	0.001
Laser beam divergence (mrad)	0.5

Figure 2.   Site of the LiDAR data.

3.2   *The optical data and its preprocessing*

Besides the airborne LiDAR data, spaceborne sensor data of SPOT-5 were acquired for the same site. With the high-resolution DEM of 0.5 m spatial resolution extracted from the LiDAR data, we have highly orthorectified the SPOT-5 high-resolution geometry (HRG) image using the method of the strict satellite imaging model. The result of the orthorectification is shown in figure 3. Both the DEM and SPOT-5 data are in the projection system of UTM Zone 47N/WGS-84.

Then the fast line-of-fight atmospheric analysis of spectral hypercubes (FLAASH) model (Matthew *et al*. 2003) was applied to the atmospheric correction of the orthorectified SPOT-5 image. The reflectance of the coniferous forest pixels in the study area changed a lot compared with those before atmospheric correction (figure 4). The reflectance values in the two visible range bands became smaller, while in the near-infrared and shortwave infrared they became larger.

The undulating topography of the study area is relatively large, which resulted in inconsistency between the measurements of the sensor and the actual spectrum values, reduced the quality of the remote-sensing images and induced many errors in the retrieval of surface parameters. Therefore, topographic correction of a remote-sensing image in forested areas is an important step in the retrieval of forest parameters. We generated slope and aspect maps (figure 5) of the study area with the DEM extracted from the LiDAR data. Then, by combining the slope and aspect maps with the solar zenith angle and the azimuth angle provided by the optical image data, we topographically corrected the SPOT-5 data. Figure 6 is a false colour composite of the SPOT-5 image after topographic correction.
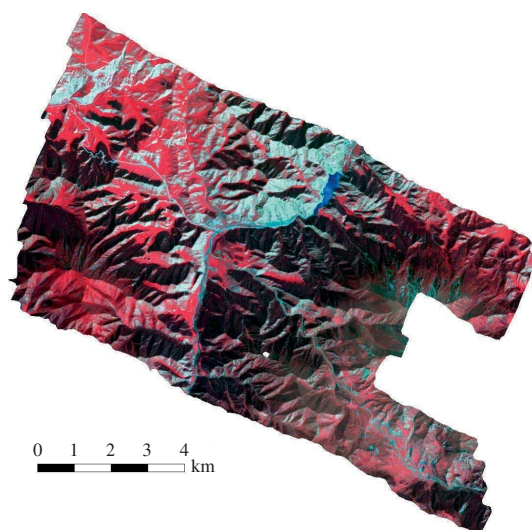
Figure 3.   False colour composite of the SPOT-5 image in the study area after orthorectification (R: XS3, G: XS2, B: XS1).
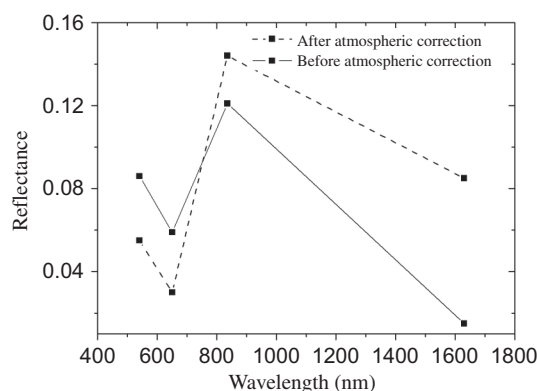

Figure 4.   Spectral change before and after atmospheric correction.

3.3   *Field inventory*

In June 2008, we took hemispherical photographs as field samples using a Nikon Coolpix 8400 (Nikon Corporation, Tokyo, Japan) with an FC-E9 adapter lens. The measurements were performed under overcast conditions to minimize the effect of sky radiance on the digital image. Hemispherical photographs of a total of 15 plots were taken and their locations were measured using differential GPS equipment (Leica, Hermeskeil, Germany). In each subplot, hemispherical photographs were taken at five measuring points, which are shown as red points in figure 7, and the average value was taken for the subplot after necessary processing. The hemispherical photographs were analysed using Gap Light Analyzer software (Simon Fraser University, Burnaby, BC, Canada). Gap fractions were computed for zenith angles 0–90° with an interval of 5° and averaged over all azimuth angles.
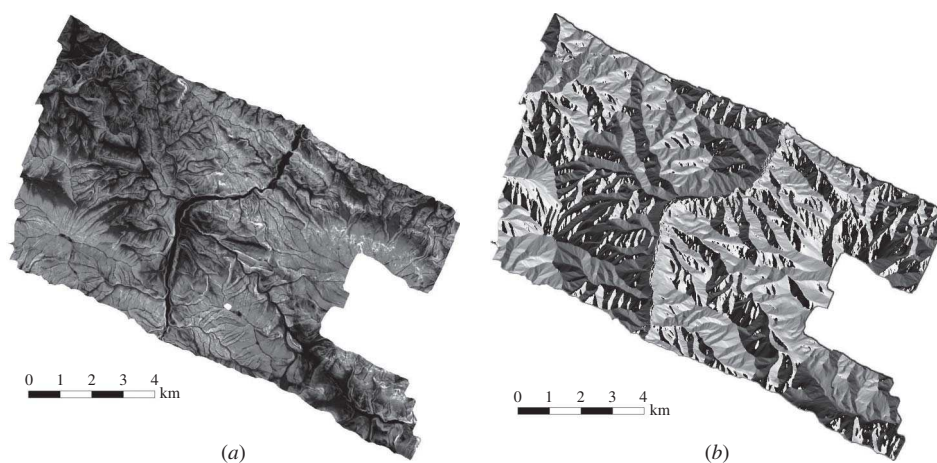
(*a*)   (*b*)

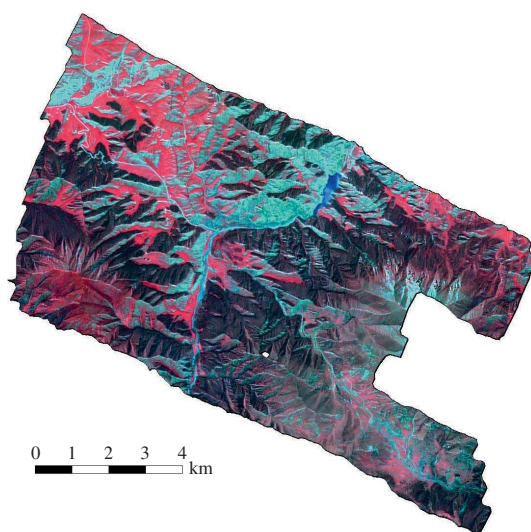Figure 5.   Slope and aspect maps of the study area: (*a*) slope map and (*b*) aspect map.

Figure 6.   False colour composite of the SPOT-5 image after topographic correction.

Besides, LAI was measured by an LAI-2000 (LI-COR Inc., Lincoln, NE, USA)
and TRAC (Canada Centre for Remote Sensing, Ottawa, ON, Canada). The LAI-
2000 was also used under overcast conditions and the measuring points were the same
as those of Hemiview measurements. The average of the five values was taken for each
subplot.

The TRAC was used in sunny conditions with sufficient direct light and no cloud.
To get the best effects, the measuring track in each plot was made perpendicular to
the line of direct solar radiation. In figure 7, the two blue lines indicate the measuring
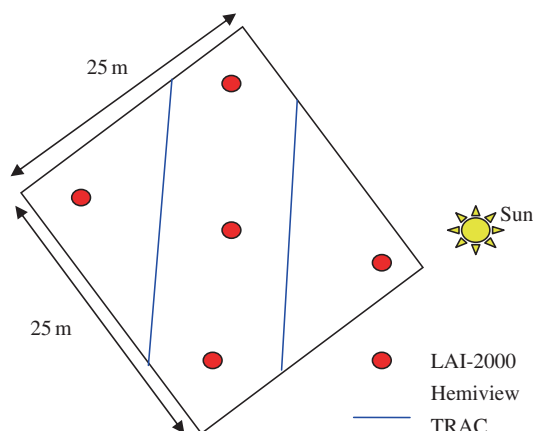tracks and their values represent the LAI for the whole subplot.

Figure 7.   Sketch map of LAI measurement using an LAI-2000, Hemiview and TRAC.

4.   Methodology

4.1   *Li–Strahler geometric-optical model*

The Li–Strahler geometric-optical model (Li and Strahler 1985, 1986, 1992), which was first developed to retrieve crown canopy and density, has been widely used in the retrieval of the vegetation structure parameters (Franklin and Strahler 1988, Franklin and Turner 1992, Woodcock *et al*. 1997, Zeng *et al*. 2008). The Li–Strahler geometric-optical model takes the pixel reflectance as an area-weighted sum of the reflectances of the four spectral scene components:

$$S = K_c C + K_g G + K_t T + K_z Z. \tag{2}$$

In this equation, C, G, T and Z are, respectively, the reflectance of a unit area of illuminated crown, illuminated background, shadowed crown and shadowed background. K_g is the proportion of the pixel not covered by crown or shadow; K_c is the proportion of area not covered by crown or shadow, that is, in an illuminated crown; K_t is the proportion of covered area in shadowed crown; and K_z is the proportion of covered area in shadowed background. As the species of plants in the study area is a single coniferous tree (*P. crassifolia*), we regarded the shape of canopy as an ellipse, which is propitious for the retrieval of forest parameters using the Li–Strahler geometric-optical model.

The forest parameters retrieved from the LiDAR data were regarded as the input parameter in the Li–Strahler geometric-optical model, and then were combined with optical images to retrieve the forest canopy cover and PAI$_e$. The flow of synchronous retrieval is shown in figure 8. The synchronous retrieval approach can be divided into three parts: (1) calculate the proportion of area not covered by crown or shadow, that is, in the illuminated background K_g using the forest parameters in the sample plot extracted from airborne LiDAR data; (2) calculate the reflectance of the illuminated background G and the average reflectance of the other scene components X_0 using a linear spectrum decomposition model according to the value of K_g and surface reflectance extracted from the SPOT-5 HRG image; and (3) incorporate the reflectances of the two end members obtained from step (2) into the Li–Strahler geometric-optical model and calculate the proportion of the pixel not covered by
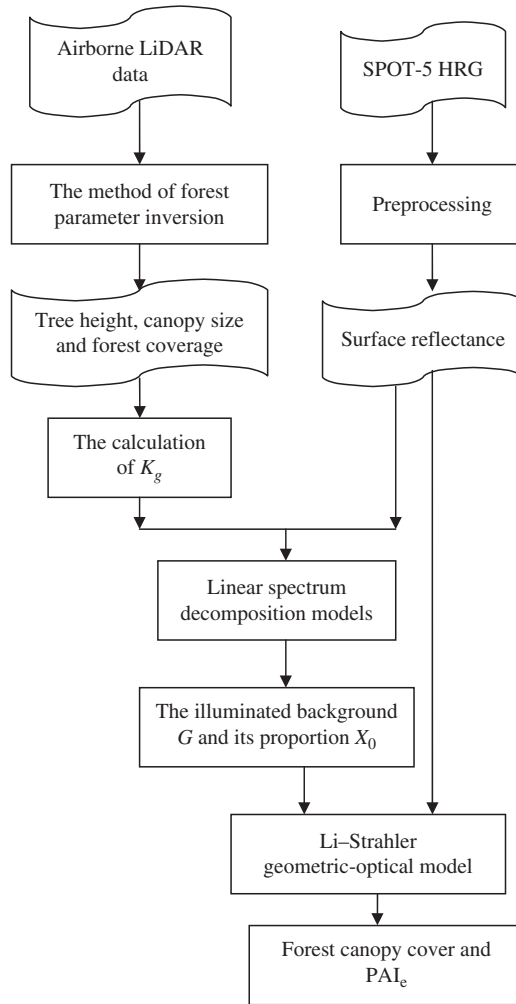
Figure 8.   Flow of synchronous retrieval.

crown or shadow K_g for each pixel in the image of the whole study area. Then, acquire the canopy coverage and PAI_e of each pixel according to K_g.

4.2   *Determination of* K_g

First, calculate the proportion of the pixel not covered by crown or shadow K_g using the Li–Strahler geometric-optical model and forest parameters such as the tree height, canopy crown and canopy coverage retrieved by airborne LiDAR data. The equation is

$$K_g = \exp\left\{-\pi m\left[\sec\theta_i' + \sec\theta_v' - O(\theta_i, \theta_v, \phi)\right]\right\}, \tag{3}$$

where θ_i and θ_v represent the solar and satellite zenith angles; ϕ is the relative azimuth angle between the sun and the satellite; and $O(\theta_i, \theta_v, \phi)$ is the overlapping part of the

illuminated shadow and the observational shadow, which is called the overlapping function. It can be calculated by the following equation:

$$O(\theta_i, \theta_v, \phi) = \frac{(t - \sin t \cos t)(\sec \theta_i' \sec \theta_v')}{\pi}, \tag{4}$$

where

$$\cos t = \frac{h}{b} \frac{\sqrt{D^2 + (\tan \theta_i' \tan \theta_v' \sin \phi)^2}}{\sec \theta_i' + \sec \theta_v'}, \tag{5}$$

$$D = \sqrt{\tan^2 \theta_i' + \tan^2 \theta_v' - 2 \tan \theta_i' \tan \theta_v' \cos \phi}, \tag{6}$$

$$\tan \theta' = \frac{b}{r} \tan \theta. \tag{7}$$

The parameters h, b and r in equations (5) and (7) individually express the average tree height, the average long radius and the average short radius of the crown in the pixel. These variables were retrieved by the LiDAR data or by measured data.

In equation (3), the parameter m is called 'treeness', which is a very important parameter that relates the remote-sensing image signal with the forest parameters (Woodcock *et al.* 1997). It expresses the average canopy coverage in the sample when the trees have no overlap. It is the function of the tree density λ and the average canopy radius r:

$$m = \lambda r^2. \tag{8}$$

When we calculate the proportion of the four scene components, according to the actual situation of the study area, we suppose the trees in the sample are distributed randomly and have no overlap. The relationship between canopy coverage and tree density and crown size can be expressed by the following equation (Li and Strahler 1985, Woodcock *et al.* 1997):

$$CC = 1 - e^{-\pi m}. \tag{9}$$

The variable m affects the calculations of the proportion of the pixel not covered by crown or shadow and the reflectance of the illuminated background, which will finally improve the precision of the model of forest parameter inversion. Equation (9) depicts the area covered by crowns and shadows, as a function of m, which is the proportion of area covered by crowns and shadows without overlapping. We can calculate the variable m using the canopy coverage in the sample plot, which can be easily retrieved by the LiDAR data. And then the proportion of pixel not covered by crown or shadow K_g can be calculated.

4.3 *Decomposition of the linear spectrum*

The linear spectrum decomposition models consider that the spectrum of the ground reflectance is composed of spectra of several pure pixels according to the proportion of their area. It can be expressed by the following equation:

$$\rho_j = \sum_{i=1}^{k} \rho_{ij} s_i + e_j,$$

$$\sum_{i=1}^{k} s_i = 1. \tag{10}$$

The variable ρ is the reflectance of the pixel; i is the order of the pixel; and j is the order of the waveband. S_i expresses the proportion of the ith pure pixel and e_j expresses the error of the jth waveband.

In our research, we simply regard the remote-sensing signal of the mixed pixel as a dimidiate component model:

$$S = K_g G + (1 - K_g) X_0, \tag{11}$$

where G represents the illuminated background and X_0 is the total of the other scene components except the illuminated background.

The reflectances of the two end members were calculated using the method of factor analysis. We first explored the proportion of the area of the end member (K_g) in the small sample plot using the high-precision tree parameters retrieved by the airborne LiDAR data, and obtained the mixed reflectivity (the variable S in equation (11)) of the corresponding pixel from the SPOT-5 image at the same time. Based on the simplified linear spectrum decomposition model (equation (11)), we established an equation set, further solved it through the method of least-square regression and thus obtained the reflectances of the two end members (G and X_0).

4.4 *Inversion of the forest canopy cover and PAI$_e$ using the Li–Strahler geometric-optical model*

With the reflectances of the two end members in the pixel (G and X_0) and the pixel reflectance of the SPOT-5 image, the proportion of the pixel not covered by crown or shadow (K_g) of the whole study area can be calculated using the simplified Li–Strahler geometric-optical model equation (11). Then, the variable m is obtained by the following equation:

$$m = \frac{-\ln(K_g)}{(\sec \theta_i + \sec \theta_v)(\pi - t + \cos t \sin t)}. \tag{12}$$

And finally, the vegetation coverage is calculated by equation (9).

The canopy gap fraction is a variable which describes the probability of interaction between light and leaves or other canopy components when it travels through the canopy. Thus, the directional canopy gap fraction describes this probability in a specific direction and generally it can be expressed as follows:

$$P(\theta_v, \varphi_v) = e^{-G(\theta_v, \varphi_v)\Omega \text{LAI} / \cos \theta_v}, \tag{13}$$

where θ_v is the view zenith angle; φ_v is the view azimuth angle; $G(\theta_v, \varphi_v)$ expresses the projected leaf area per unit area in the observed direction; LAI is the real leaf

area index; and Ω is the clumping index, which is equal to 1 when the leaves are randomly distributed (Lemeur and Blad 1974). The equation indicates that the probability of interaction between light and leaves or other canopy components has a negative exponential relationship with the actual leaf area in the observed direction.

According to Monsi and Saeki (2005), light attenuation in the vegetation canopy is related to canopy structure and LAI. As the leaves and the branches have not been distinguished in this article and the clumping situation in the canopy is also beyond consideration, the concept of PAI_e is used here. Then, based on the Beer–Lambert law, we can express equation (13) as follows:

$$I = I_0 e^{-K PAI_e}, \tag{14}$$

where I expresses the radiation intensity of light which penetrates the canopy; I_0 expresses the radiation intensity of light on top of the canopy; PAI_e is the effective plant area index; and K is the extinction coefficient, which is affected by many factors such as leaf inclination angle distribution, radiation type, canopy structure, clumping index and so on (Breda 2003). K can be expressed as follows:

$$K(\theta) = \frac{G(\theta)\Omega(\theta)}{\cos \theta}, \tag{15}$$

where θ is the zenith angle. If we assume that the leaf inclination angle distribution of *P. crassifolia*, which is the main tree species in our study area, is spherical in distribution ($G(\theta) = 0.5$), the airborne LiDAR is approximately the vertical viewing angle ($\cos \theta \approx 1$) and the leaves are randomly distributed ($\Omega(\theta) = 1$), then K is approximately equal to 0.5.

If we take the incident laser beam P_0 as the light radiation on top of the canopy I_0, and the laser beam P_g which travels through the canopy to the ground as the light radiation which penetrates the canopy I, then equation (14) can be rewritten as

$$P_g = P_0 e^{-K PAI_e}, \tag{16}$$

where K can be understood as the interception coefficient of canopy to laser beam, which can also be expressed by equation (15).

As the scanning angle of airborne LiDAR is quite small and the laser beam is approximately vertically incident on the surface, we can express the canopy cover as follows:

$$CC = 1 - \frac{P_g}{P_0}. \tag{17}$$

This can be rewritten as

$$1 - CC = e^{-K PAI_e}. \tag{18}$$

Using some transformation, we can acquire the retrieval equation of PAI_e:

$$PAI_e = -\frac{\ln(1 - CC)}{K}. \tag{19}$$

Substituting equation (9) in equation (19), the relationship between PAI$_e$ and the variable *m* can be expressed as

$$\text{PAI}_e \approx -2\ln(\text{e}^{-\pi m}) = 2\pi m. \tag{20}$$

From equations (12) and (20), we can see that there is a negative logarithmic relationship between PAI$_e$ and the proportion of the pixel not covered by crown or shadow K_g. It is the same as the conclusion acquired by Hu *et al.* (2004), wherein they think there is a negative logarithmic relationship between the canopy LAI and the proportion of the pixel not covered by crown or shadow (i.e. covered by snow). We use this conclusion to retrieve the PAI$_e$ in our study area.

5. Retrieval and validation of forest canopy cover and PAI$_e$

5.1 *Retrieval and validation of forest canopy cover*

Using the above synergy inversion algorithm, we input the forest parameters which were extracted from the LiDAR data into the Li–Strahler geometric-optical model synchronously using the SPOT-5 HRG data to calculate the proportion of the pixel not covered by crown or shadow K_g. Figure 9 shows the extracted image of K_g, in which the white areas include bare ground, grassland and some non-value areas. With the extracted variable K_g, we can easily retrieve the forest canopy cover according to equations (12) and (9). As shown in figure 10, the light green areas indicate a low forest canopy cover, while the deep green areas indicate a high forest canopy cover.

Since we do not have the simultaneous ground measurements, the forest canopy cover measured by Hemiview in June 2008, which is 2 months earlier than the SPOT-5 data, was used to validate the result. The sample of Hemiview measured data is 25 m × 25 m in size, while the retrieved image has a spatial resolution of 10 m × 10 m. So the retrieved image must be resampled to a spatial resolution of 25 m and then
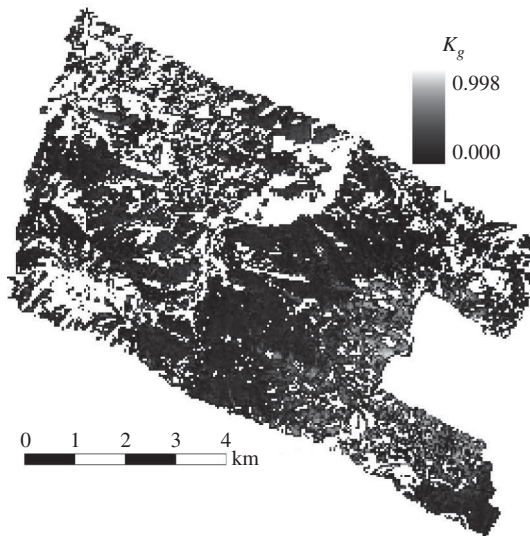

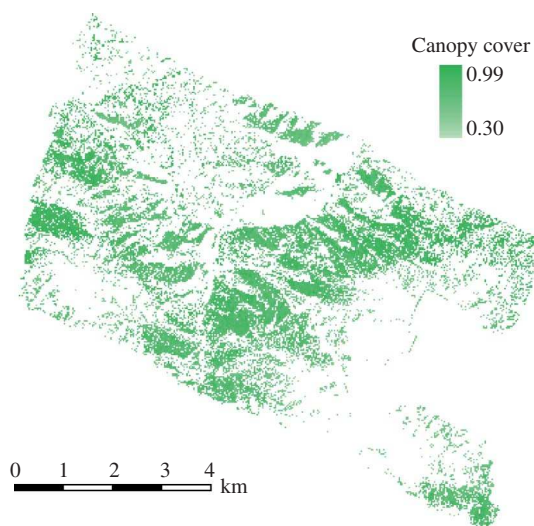Figure 9.   Areal proportion of sunlit ground within each pixel.

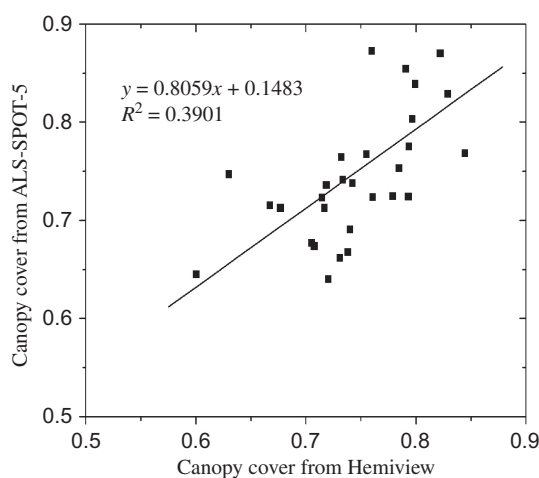Figure 10.   Retrieval results of forest canopy cover.

$y = 0.8059x + 0.1483$
$R^2 = 0.3901$

Figure 11.   Comparison of forest canopy cover from ALS-SPOT-5 and Hemiview.

compared with the measured data. As shown in figure 11, the R^2 between retrieved data and measured data is 0.3901. This is mainly because the acquired time of the SPOT-5 image and the measured data has a discrepancy of about 2 months, which causes many errors. Therefore, the retrieved result needs further validation. However, the error bars of forest canopy cover from Hemiview and LiDAR–SPOT-5 (figure 12) show that the average values from the two approaches are approximately the same, which indicates some degree of efficiency. Compared with the retrieved result, the values from Hemiview are less volatile and concentrated in a relatively narrow range. This may result for many reasons, among which the following are possible. First, the Hemiview must be used under overcast conditions, which make it easily influenced by diffusion light, and the dense vegetation enhances this effect. And then the large undulating terrain has an impact on the measurement of Hemiview. Finally, the traditional
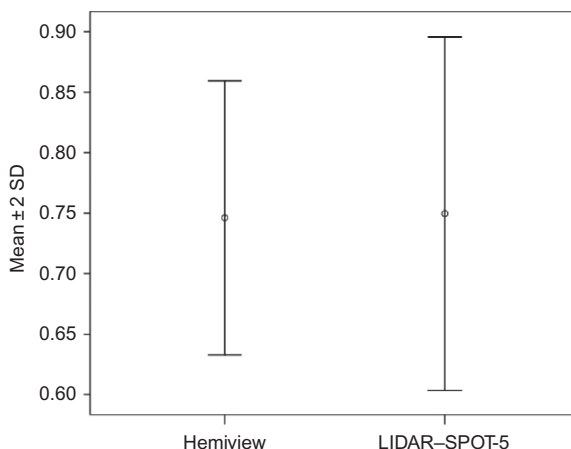
Figure 12. Error bars of forest canopy cover from Hemiview and LiDAR–SPOT-5.

processing function chosen using Gap Light Analyzer software during the processing of hemispherical photographs may result in the underestimation of forest cover.

5.2 *Retrieval and validation of PAI$_e$*

We can retrieve the PAI$_e$ of the study area using the above retrieved forest canopy cover, according to equation (20). The result is shown in figure 13, in which the PAI$_e$ of the whole study area ranges from 0.7 to 8.99; most values are between 1 and 6. We validate the retrieved PAI$_e$, respectively, using the TRAC and LAI-2000 measurements. We still need to resample the retrieved result to a spatial resolution of 25 m. The result shows that the R^2 are, respectively, 0.5173 and 0.7471, which indicates the efficiency of our methods (see figures 14 and 15). In figure 16, we find that compared with the synchronous retrieval result, the values from the LAI-2000 are smaller and the
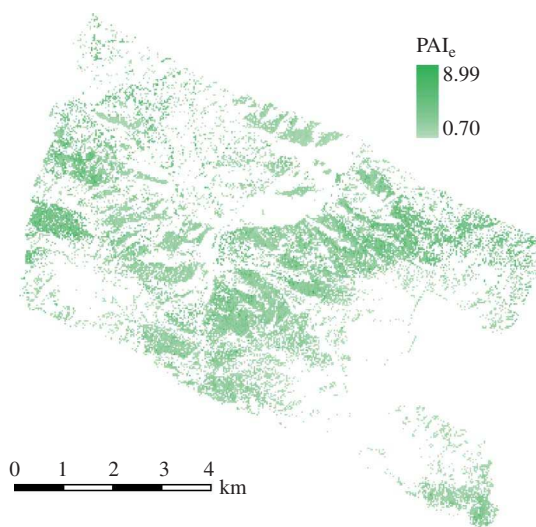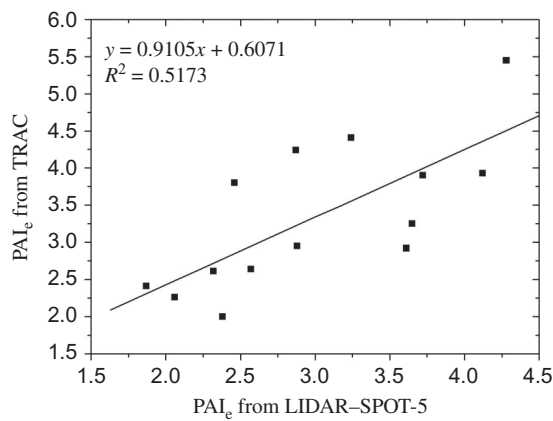

Figure 13. Retrieval results of PAI$_e$.

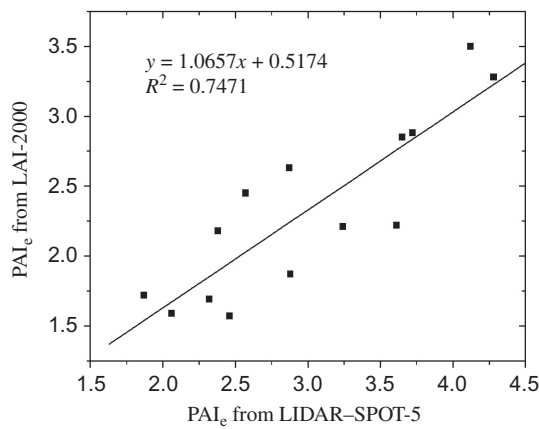Figure 14. Comparison of PAI_e from LiDAR–SPOT-5 and TRAC.

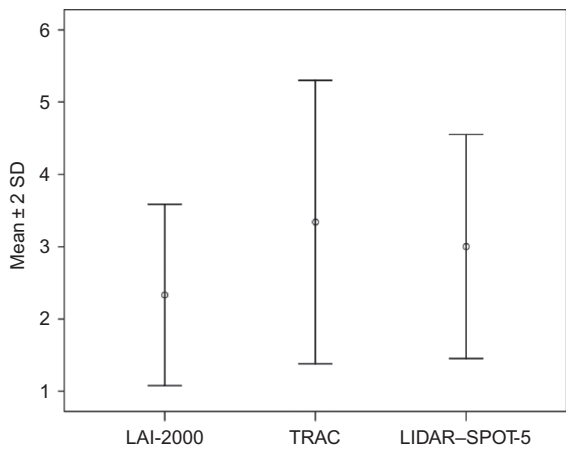Figure 15. Comparison of PAI_e from LiDAR–SPOT-5 and LAI-2000.

Figure 16. Error bars of PAI_e from LAI-2000, TRAC and LiDAR–SPOT-5.

TRAC-measured values are larger. These may relate to their measurement principles, methods and so on, which need further research.

6.   Conclusion

This article proposed to retrieve forest structure parameters using LiDAR data, and used a linear spectrum decomposition model to determine the reflectances of the spectral scene components, which are regarded as prior knowledge in the retrieval of forest canopy cover and PAI$_e$ using a simplified Li–Strahler geometric-optical model. Airborne LiDAR data are first used to retrieve forest structure parameters and then the proportion of the pixel not covered by crown or shadow K_g for each pixel in the sample was calculated, which was used to extract the reflectances of the spectral scene components by a linear spectrum decomposition model. And finally the forest canopy cover and PAI$_e$ were retrieved by the geometric-optical model. As the acquired time of the SPOT-5 image and measured data has a discrepancy of about 2 months, the retrieved result of forest canopy cover needs a further validation. The relatively high value of R^2 between the retrieval result of PAI$_e$ and the measurements indicates the efficiency of our methods.

References
BAO, Y.F., CAO, C.X., ZHANG, H., CHEN, E.X., HE, Q.S., HUANG, H.B., LI, Z.Y., LI, X.W. and GONG, P., 2008, Synchronous estimation of DTM and fractional vegetation cover in forested area from airborne LIDAR height and intensity data. *Science in China Series E*, **51**, pp. 176–187.
BREDA, N.J.J., 2003, Ground-based measurements of leaf area index: a review of methods, instruments and current controversies. *Journal of Experimental Botany*, **54**, pp. 2402–2417.
CHOPPING, M., MOISEN, G.G., SU, L., LALIBERTE, A., RANGO, A., MARTONCHIK, J.V. and PETERS, D.P.C., 2008, Large area mapping of southwestern forest crown cover, canopy height, and biomass using the NASA Multiangle Imaging Spectro-Radiometer. *Remote-sensing of Environment*, **112**, pp. 2051–2063.
CHOPPING, M., SU, L., LALIBERTE, A., RANGO, A. and PETERS, D.P.C., 2006, Mapping shrub abundance in desert grasslands using geometric-optical modeling and multi-angle remote-sensing with CHRIS/PROBA. *Remote-sensing of Environment*, **104**, pp. 412–422.
FRANKLIN, J. and STRAHLER, A.H., 1988, Invertible canopy reflectance modeling of vegetation structure in semiarid woodland. *IEEE Transactions on Geoscience and remote-sensing*, **26**, pp. 809–825.
FRANKLIN, J. and TURNER, D.L., 1992, The application of a geometric optical canopy reflectance model to semiarid shrub vegetation. *IEEE Transactions on Geoscience and remote-sensing*, **30**, pp. 293–301.

HALL, F.G., SHIMABUKURO, Y.E. and HUEMMRICH, K.F., 1995a, remote-sensing of forest biophysical structure using mixture decomposition and geometric reflectance model. *Ecological Applications*, **5**, pp. 993–1013.

HALL, F.G., TOWNSHEND, J.R. and ENGMAN, E.T., 1995b, Status of remote-sensing algorithms for estimation of land surface state parameters. *Remote-sensing of Environment*, **51**, pp. 138–156.

HU, B., MILLER, J.R., CHEN, J.M. and HOLLINGER, A., 2004, Retrieval of the canopy leaf area index in the BOREAS flux tower sites using linear spectral mixture analysis. *Remote-sensing of Environment*, **89**, pp. 176–188.

LEMEUR, R. and BLAD, B.L., 1974, A critical review of light models for estimating the shortwave radiation regime of plant canopies. *Agriculture and Forest Meteorology*, **14**, pp. 255–286.

LI, X. and STRAHLER, A.H., 1985, Geometric-optical modeling of a conifer forest canopy. *IEEE Transactions on Geoscience and remote-sensing*, **GE 23**, pp. 705–721.

LI, X. and STRAHLER, A.H., 1986, Geometric-optical bidirectional reflectance modeling of a conifer forest canopy. *IEEE Transactions on Geoscience and remote-sensing*, **GE 24**, pp. 906–919.

LI, X. and STRAHLER, A.H., 1992, Geometric-optical bidirectional reflectance modeling of the discrete crown vegetation canopy: effect of crown shape and mutual shadowing. *IEEE Transactions on Geoscience and remote-sensing*, **30**, pp. 276–292.

MATTHEW, M.W., ALDLER-COLDEN, S.M., BERK, A., FELDE, G., ANDERSO, G.P., GORODESTZKY, D., PASWATERS, S. and SHIPPERT, M., 2003, Atmospheric correction of spectral imagery: evaluation of the FLAASH algorithm with AVIRIS data. In *SPIE Proceeding, Algorithm and Technologies for Multispectral, Hyperspectral, and Ultraspectral Imagery IX*, April 2003, Bellingham, WA.

MONSI, M. and SAEKI, T., 2005, On the factor light in plant communities and its importance for matter production (an English translation of Monsi and Saeki (1953)). *Annals of Botany*, **95**, pp. 549–567.

POPESCU, S.C., WYNNE, R.H. and NELSON, R.E., 2002, Estimating plot-level tree heights with lidar: local filtering with a canopy-height based variable window. *Computers and Electronics in Agriculture*, **37**, pp. 71–95.

WOODCOCK, C.E., COLLINS, J.B., JAKABHAZY, V.D., LI, X., MACOMBER, S.A. and WU, Y., 1997, Inversion of the Li–Strahler canopy reflectance model for mapping forest structure. *IEEE Transactions on Geoscience and remote-sensing*, **35**, pp. 405–414.

ZENG, Y., SCHAEPMAN, M.E., WU, B., CLEVERS, J.G.P.W. and BREGT, A.K., 2008, Scaling-based forest structural change detection using an inverted geometric-optical model in the Three Gorges region of China. *Remote-sensing of Environment*, **112**, pp. 4261–4271.